

Granular hopping conduction in $(\text{Ag},\text{Mo})_x(\text{SnO}_2)_{1-x}$ films in the dielectric regime

Ya-Nan Wu, Yan-Fang Wei, and Zhi-Qing Li*

*Tianjin Key Laboratory of Low Dimensional Materials Physics and Preparing Technology,
Department of Physics, Tianjin University, Tianjin 300072, China*

Juhn-Jong Lin†

*Institute of Physics and Department of Electrophysics,
National Chiao Tung University, Hsinchu 30010, Taiwan*

We have studied the temperature dependence of conductivity, $\sigma(T)$, in two series of $\text{Ag}_x(\text{SnO}_2)_{1-x}$ and $\text{Mo}_x(\text{SnO}_2)_{1-x}$ granular films lying below the percolation threshold, where x is the metal volume fraction. The metal grains in the former series have approximately spherical shape, whereas in the latter series contain numerous small substructures. In both series of films, we have observed the $\sigma \propto \exp[-(T_0/T)^m]$ temperature dependence, with $m \simeq 1/2$, over the wide T range from 2 to 80 (100) K, where T_0 is a characteristic temperature. Our $\sigma(T)$ results are explained in term of the Abeles-Sheng model which considers the structural effect of metal grains. The extracted values of the optimal separation between grains (s_m) and the charging energy (E_c) slightly increase with decreasing x . The variation of the parameter $C(x)$, defined in the Abeles-Sheng model, is in consistency with a simplified expression which depends only on x and the dielectric constant of the insulating matrix. As the temperature is increased to above ~ 100 K, a crossover to the thermally fluctuation-induced tunneling conduction processes is observed.

Keywords: granular hopping conduction, dielectric regime, metal-insulator composites, percolation

I. INTRODUCTION

Granular metals, M_xI_{1-x} , are composite mixtures composed of nanometer-sized metal particles embedded in a dielectric matrix, where M denotes a metal, I denotes an insulator, and x denotes the metal volume fraction. Due to the specific nanoscale structure, granular metals reveal novel physical properties that are not found in homogeneous systems.¹ For instance, the electron-electron interaction effect on the transport properties in the presence of granularity has been demonstrated to be significantly different from those in homogeneous disordered metals.^{2,3} A $\ln(T)$ temperature dependence of conductivity and Hall coefficient was observed to be independent of granular array dimensionality. The transport properties of granular systems in the dielectric regime ($x < x_c$, the percolation threshold) are expected to be distinctive as well. Very often, the following temperature dependence of electrical conductivity, σ , is observed over an extended range of T :⁴⁻¹⁸

$$\sigma(T) = \sigma_0 \exp \left[- (T_0/T)^{1/2} \right], \quad (1)$$

where σ_0 and T_0 are sample dependent parameters. On the other hand, the T dependence as described by the form of Eq. (1) has also been widely observed in amorphous and doped crystalline semiconductors, and satisfactorily explained by the Efros-Shklovskii variable-range-hopping (VRH) conduction processes in the presence of a Coulomb gap.¹⁹⁻²³

As early as in the 1970s, Abeles, Sheng and coworkers have explored this kind of stretched-exponential $\sigma(T)$ behavior, Eq. (1), by considering the structural effects of constituting metal grains.²⁴⁻²⁶ They have noted that charge carriers are generated by thermal activation

and transferred by tunneling between neighboring grains. The tunneling takes place along certain optimal percolation paths. The selection of optimal paths is based on an assumption that the ratio s/a is a function of x alone, where s is the separation between neighboring metal grains, and a is the metal grain size. This theory has been successfully used to explain the results in a number of granular systems that have a distribution of a .⁵⁻⁷ However, it has also been argued that the Abeles-Sheng model is inappropriate to account for the observations in other granular systems.^{11,27,28} Multiple theoretical models aiming at clarifying the robust $\sigma \propto \exp[-(T_0/T)^{1/2}]$ behavior have been put forward over years, but a full theory has yet to be achieved.¹²⁻¹⁵ Recently, a correlated hopping mechanism based on multiple co-tunneling processes has been formulated, where the electrostatic disorder induced by charged traps in the insulating matrix is predicted to cause the form of Eq. (1).²⁹ The validity of this co-tunneling model awaits experimental tests.

To clarify this long-standing problem, we study the $\sigma(T)$ behaviors of two series of $\text{Ag}_x(\text{SnO}_2)_{1-x}$ and $\text{Mo}_x(\text{SnO}_2)_{1-x}$ granular films in this work. The first series of films contains approximately spherical metal grains with a grain size distribution smaller than $\approx 40\%$. The second series of films has small substructures in the Mo grains. The electronic transport properties for these films in the metallic regime ($x > x_c$) were reported previously.^{30,31} We point out that the percolation threshold is $x_{Ag}^c \simeq 0.50$ in the $\text{Ag}_x(\text{SnO}_2)_{1-x}$ films and $x_{Mo}^c \simeq 0.32$ in the $\text{Mo}_x(\text{SnO}_2)_{1-x}$ films.

II. EXPERIMENTAL METHOD

The cosputtering fabrication method for our samples was described previously.^{30,31} The thickness of the films was determined by a surface profiler (Dektak, 6 M). The $\text{Ag}_x(\text{SnO}_2)_{1-x}$ films were ≈ 500 nm thick, and $\text{Mo}_x(\text{SnO}_2)_{1-x}$ films were ≈ 350 nm thick. The Ag (Mo) volume fraction x in each sample was obtained from the energy-dispersive x-ray spectroscopy analysis. The microstructure of the films was studied by the transmission electron microscopy (TEM, Tecnai G2 F20). The electrical measurements were performed on a physical property measurement system (PPMS-6000, Quantum Design), employing the four-probe technique.

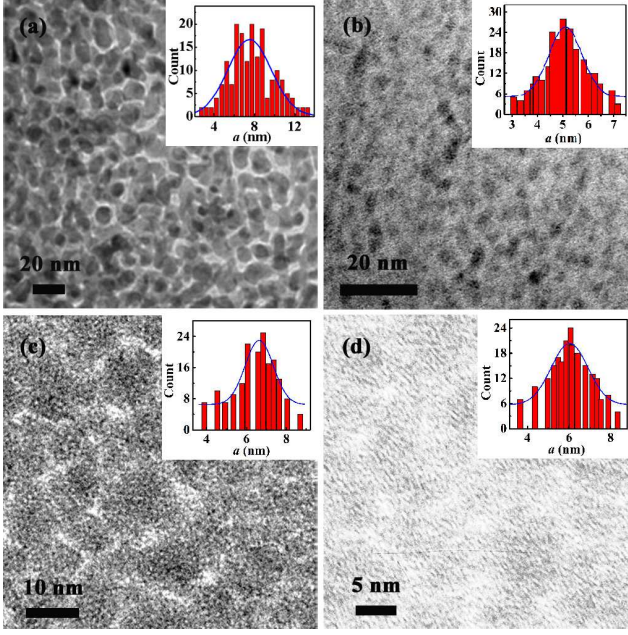


FIG. 1. TEM images for $\text{Ag}_x(\text{SnO}_2)_{1-x}$ films with (a) $x \approx 0.62$ (taken from Ref. 3), and (b) ≈ 0.26 (taken from Ref. 30); and for $\text{Mo}_x(\text{SnO}_2)_{1-x}$ films with (c) $x \approx 0.36$, and (d) ≈ 0.29 [(c) and (d) are taken from Ref. 31]. The inset in each panel shows the corresponding grain size distribution histogram. The percolation thresholds are $x_{\text{Ag}}^c \approx 0.50$ and $x_{\text{Mo}}^c \approx 0.32$ in $\text{Ag}_x(\text{SnO}_2)_{1-x}$ and $\text{Mo}_x(\text{SnO}_2)_{1-x}$ films, respectively.

III. RESULTS AND DISCUSSION

Figure 1 shows representative TEM images for two $\text{Ag}_x(\text{SnO}_2)_{1-x}$ films and two $\text{Mo}_x(\text{SnO}_2)_{1-x}$ films, with x as indicated in the caption to Fig. 1. The inset in each panel shows the corresponding grain size distribution histogram. We note that the two series of films have distinct metal grain structures. The $\text{Ag}_x(\text{SnO}_2)_{1-x}$ films reveal typical granular characteristics.³⁰ The Ag particles are approximately spherical in shape and embedded in the

amorphous SnO_2 matrix, with well-defined metal grain boundaries. On the other hand, in the $\text{Mo}_x(\text{SnO}_2)_{1-x}$ films, there are no regularly shaped Mo grain boundaries. Both Mo and SnO_2 particles reveal small substructures penetrating into each other.³¹ Selected-area diffraction patterns indicate that the Ag grains are crystalline,^{3,30} whereas the Mo grains are amorphous.³¹ The mean grain size of Ag and Mo grains in $\text{Ag}_x(\text{SnO}_2)_{1-x}$ and $\text{Mo}_x(\text{SnO}_2)_{1-x}$ films with $x < x_c$ are $\approx 5 \pm 2$ nm and $\approx 6 \pm 4$ nm, respectively, see Figs. 1(b) and 1(d). It is worth noting that these mean grain sizes are slightly smaller than those in the films with $x > x_c$, see Figs. 1(a) and 1(c).

Assume that the temperature T dependence of conductivity can be written in the form $\sigma(T) = \sigma_0 \exp[-(T_0/T)^m]$. We define a parameter $L(T) \equiv \partial \log_{10}(\sigma) / \partial \log_{10}(T) = -m(T_0/T)^m$, and then write $\log_{10} L(T) = \log_{10}(-mT_0^m) - m \log_{10} T$.³² That is, there exists a linear expression for $\log_{10} L$ versus $\log_{10} T$, with m as the slope. In Fig. 2, we plot the parameter L calculated from our measured $\sigma(T)$ in double logarithmic scales for both series of films, as indicated. Obviously, $\log_{10} L$ varies linearly with $\log_{10} T$ over a wide range of T for all the representative films shown in Figs. 2(a) and 2(b). We thus obtain the slopes m for each series of films and plot them in the corresponding insets. It is clearly seen that m takes a value of ≈ 0.5 , which in turn strongly suggests the validity of the $\sigma \propto \exp[-(T_0/T)^{1/2}]$ temperature law. Thus, it is well justified to perform least-squares fits of our $\sigma(T)$ data to Eq. (1). We have then extracted the values of the adjusting parameters σ_0 and T_0 for each film, as listed in Table I.

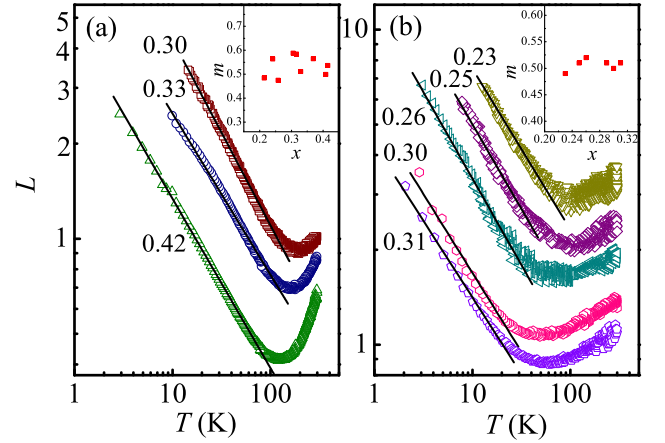


FIG. 2. Parameter L versus T in log-log scales for several (a) Ag-SnO₂ films, and (b) Mo-SnO₂ films, with the metal volume fraction x as indicated. The solid straight lines are linear fits. Insets: The fitted slope m as a function of x for each series of films.

TABLE I. Relevant parameters for $\text{Ag}_x(\text{SnO}_2)_{1-x}$ and $\text{Mo}_x(\text{SnO}_2)_{1-x}$ films. σ_0 and T_0 are defined in Eq. (1), T_1 and T_{0F} are defined in Eq. (5), and ϕ_0 (w) is the barrier height (width) computed from Eqs. (6) and (7) by setting the effective barrier area $A \approx 3 \text{ nm}^2$.

	x	$\sigma(300 \text{ K})$ (S/m)	σ_0 (S/m)	T_0 (K)	T_1 (K)	T_{0F} (K)	ϕ_0 (meV)	w (Å)
Ag series	0.21	132	415	728	2018	341	145	19.3
	0.24	126	442	679	1825	333	135	18.5
	0.28	288	1598	727	1538	331	118	16.8
	0.30	848	3912	613	794	207	84.1	16.4
	0.31	779	3085	445	793	236	79.8	14.8
	0.33	1506	3248	245	816	267	77.7	13.6
	0.37	1760	3942	199	720	276	69.4	12.3
	0.41	2973	4144	77.4	652	297	62.3	10.9
Mo series	0.42	3133	4459	71.3	610	294	59.2	10.6
	0.23	74.8	183	2056	2706	214	222	33.4
	0.25	170	259	942	2205	239	180	27.1
	0.26	662	661	470	1443	198	138	24.4
	0.29	574	442	465	1352	181	136	25.2
	0.30	1337	597	107	1241	237	114	19.3
	0.31	2528	1657	88.2	827	203	87.6	17.1

A. Comparison with the Abeles-Sheng model

In the Abeles-Sheng model, the T dependence of conductivity originates from the optimization of the product of mobility and density of charges over all percolation paths. Abeles and Sheng have defined the parameter $C \equiv \chi s E_c$, where $\chi = \sqrt{2m\phi/\hbar^2}$ is a constant related to the effective barrier height ϕ , and E_c is the charging energy required to generate a pair of positively and negatively charged grains. Abeles and Sheng have obtained the form of Eq. (1) with the relation $C = k_B T_0/4$, where k_B is the Boltzmann constant. Thus, the value of C for a given sample is experimentally determined from the extracted value of T_0 .

Abeles and Sheng have assumed that the ratio s/a is a function of x alone. By further assuming that the metal grains are spherical and packed in a simple cubic lattice, they have obtained the expression

$$s/a = (\pi/6x)^{1/3} - 1. \quad (2)$$

They have calculated the optimal separation between neighboring grains in the percolating paths, denoted by s_m , and obtained $s_m = \sqrt{C/k_B T}/2\chi$. To compare the experimental data with their theoretical predictions, we take $\phi \approx 0.1 \text{ eV}$ in our films. This value is just the difference between the work function of Ag (Mo) $\simeq 4.6 \text{ eV}$ and the electron affinity of $\text{SnO}_2 \simeq 4.5 \text{ eV}$.^{33–36} Then, we have the estimate of $\chi = 0.16 \text{ Å}^{-1}$. The values of s_m for our films can then readily be extracted from the known values of C and χ . Figures 3(a) and 3(b) show the variation of s_m (at a representative $T = 10 \text{ K}$) with x for $\text{Ag}_x(\text{SnO}_2)_{1-x}$ and $\text{Mo}_x(\text{SnO}_2)_{1-x}$ films, respectively. We see that, in both series of films, s_m slightly increases from 0.4 to 2.2 nm with decreasing x . This

variation of s_m is in line with that previously found in other composite materials.^{7,25,33}

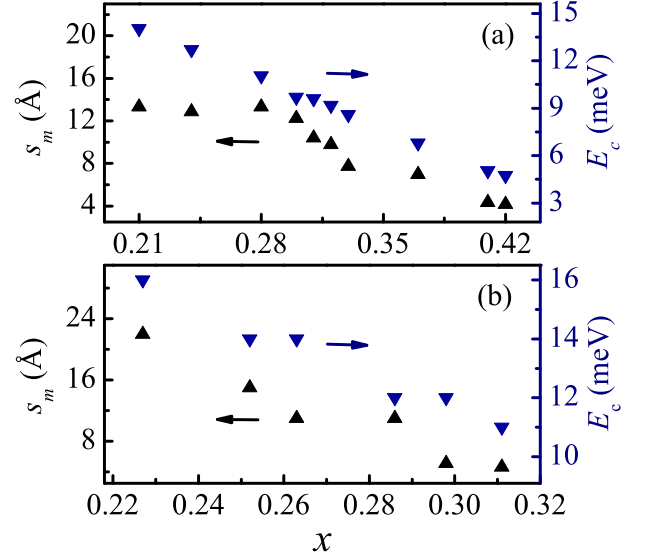


FIG. 3. Optimal separation between metal grains s_m and charging energy E_c computed from the Abeles-Sheng model for (a) $\text{Ag}_x(\text{SnO}_2)_{1-x}$ films, and (b) $\text{Mo}_x(\text{SnO}_2)_{1-x}$ films. The values of s_m are for $T = 10 \text{ K}$.

The charging energy is defined by $E_c = e^2/2\pi\epsilon_0\kappa a$, where $\kappa = \epsilon(1 + a/2s)$ is the effective dielectric constant in the granular composite, and ϵ_0 (ϵ) is the permittivity of vacuum (insulating medium). Using $\epsilon = 12$ for the amorphous SnO_2 matrix,^{37,38} we have obtained the variation of E_c with x , as also shown in Fig. 3. The typical value of E_c for those films lying just below the percolation threshold is on the order of a few meV.

The structural and composition dependent parameter C defined in the Abeles-Sheng model can be expressed in an explicit form:²⁵

$$C = \eta \frac{(s/a)^2}{(1/2) + (s/a)}, \quad (3)$$

where

$$\eta = \chi e^2/2\pi\epsilon_0\epsilon. \quad (4)$$

This parameter can provide a self-consistency check for the validity of the model, since it depends only on x and the dielectric constant of the insulating matrix. Figure 4 shows the variation of C with x for the $\text{Ag}_x(\text{SnO}_2)_{1-x}$ and $\text{Mo}_x(\text{SnO}_2)_{1-x}$ films, as indicated. The solid curve is the least-squares fit to Eq. (3) with the single adjusting parameter $\eta = 0.17 \text{ eV}$. Inspection of Fig. 4 indicates that the results for the $\text{Ag}_x(\text{SnO}_2)_{1-x}$ films can be well described by Eq. (3), whereas there is some discrepancy for the case of the $\text{Mo}_x(\text{SnO}_2)_{1-x}$ films. The discrepancy

is not unexpected. It may originate from the irregular shape of Mo grains and a relatively large distribution in grain size a .

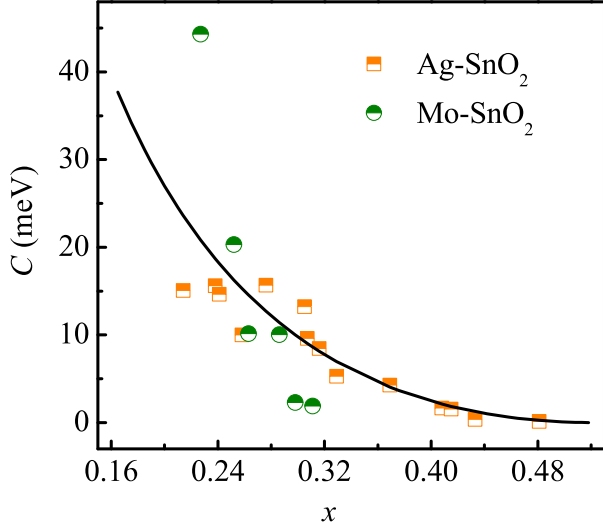


FIG. 4. Variation of parameter C with x for $\text{Ag}_x(\text{SnO}_2)_{1-x}$ and $\text{Mo}_x(\text{SnO}_2)_{1-x}$ films, as indicated. The symbols are the experimental data, and the solid curve is the prediction of Eq. (3) with $\eta = 0.17$ eV.

B. Fluctuation-induced tunneling conduction above ~ 100 K

As the temperature is increased to above ~ 100 K, our measured $\sigma(T)$ behavior crosses over to the fluctuation-induced tunneling (FIT) conduction processes. The FIT mechanism has originally been formulated for disordered systems characterized by large conducting regions separated by thin insulating barriers. In this model, the thermally induced voltage fluctuations have modulating effects on potential barriers, which play an important role in enhancing the electron tunneling probability and thereby lead to a characteristic T dependence of conductivity^{39–41}

$$\sigma(T) = \sigma_{0F} \exp \left[-\frac{T_1}{T + T_{0F}} \right], \quad (5)$$

where σ_{0F} is a weakly T dependent parameter. The characteristic temperatures T_1 and T_{0F} are defined by^{42,43}

$$T_1 = \frac{8\epsilon_0\epsilon A\phi_0^2}{k_B e^2 w}, \quad (6)$$

and

$$T_{0F} = \frac{16\epsilon_0\epsilon\hbar A\phi_0^{3/2}}{\pi(2m_e)^{1/2}k_B e^2 w^2}, \quad (7)$$

where A is the effective tunneling barrier area, m_e is the charge carrier mass, \hbar is the Planck constant divided by 2π , and ϕ_0 (w) is the insulating barrier height (width).

Figures 5(a) and 5(b) show the conductivity as a function of $1/T$ for $\text{Ag}_x(\text{SnO}_2)_{1-x}$ and $\text{Mo}_x(\text{SnO}_2)_{1-x}$ films above 40 K, respectively. The solid curves are least-squares fits to Eq. (5). Clearly, the experimental $\sigma(T)$ data for both series of films can be well described by Eq. (5) from 300 K down to ~ 100 K. In the FIT model, the size of conducting grains should be large enough such that $E_c < k_B T$. Thus, the value $T_{min} = E_c/k_B$ indicates a low-bound temperature for the FIT mechanism to be applicable. We evaluate $T_{min} \approx 110$ K for the $\text{Ag}_x(\text{SnO}_2)_{1-x}$ films and ≈ 150 K for the $\text{Mo}_x(\text{SnO}_2)_{1-x}$ films. A good agreement between this estimate and the experiment is reached for the Ag-based films, because the metal grains in this series of films have spherical shape with a fairly well defined grain size. The agreement for the Mo-based films is not as good, but still acceptable.

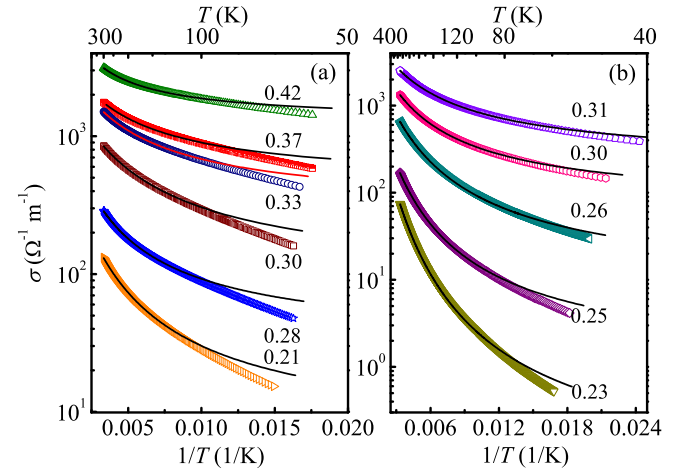


FIG. 5. Variation of conductivity with inverse temperature for several (a) $\text{Ag}_x(\text{SnO}_2)_{1-x}$ films, and (b) $\text{Mo}_x(\text{SnO}_2)_{1-x}$ films. The solid curves are least-squares fits to Eq. (5). The numbers indicate the metal volume fraction x .

According to the FIT model, most of the electron tunneling occurs within the small surface areas of metallic grains. Hence, the effective barrier area A should be given by the size of the closest approach between grains. Assuming that the value of A to be on the order of a tenth of the maximal cross section of a spherical grain, we take $A \sim 3 \text{ nm}^2$ to compute the values of ϕ_0 and w in Eqs. (6) and (7). The calculated values are listed in Table I. We see that the values of ϕ_0 and w decrease with increasing x . Our ϕ_0 values are somewhat lower than those extracted for C-PVC composites,⁴⁰ and RuO_2 and IrO_2 nanowires,⁴⁴ but compatible to those in ZnO nanowires,⁴³ micrometer-sized $\text{Al}/\text{AlO}_x/\text{Y}$ tunnel junctions,⁴⁵ and ITO films.⁴⁶ This smallness of the extracted ϕ_0 value has recently been theoretically reconsidered by Xie and Sheng.⁴⁷ On the other hand, the ex-

tracted w values are in good consistency with the s_m values extracted from the Abeles-Sheng model discussed in the above subsection, and similar to those reported for the above-mentioned materials.

IV. CONCLUSION

We have studied the electrical transport properties of two series of $\text{Ag}_x(\text{SnO}_2)_{1-x}$ and $\text{Mo}_x(\text{SnO}_2)_{1-x}$ granular films in the dielectric regime. In all films, the $\sigma \propto \exp[-(T_0/T)^{1/2}]$ temperature dependence has been observed over a wide temperature range from 2 to ~ 100 K. We explain our results within the framework of the Abeles-Sheng model that considers structural effect of

metal grains. The extracted values of the relevant parameters are in satisfactory agreement with the theory. As the temperature is increased to above about 100 K, the conductivity is governed by the thermally fluctuation-induced tunneling conduction processes.

ACKNOWLEDGMENTS

This work was supported by the National Natural Science Foundation of China (NSFC) through Grant No. 11174216 and the Research Fund for the Doctoral Program of Higher Education through Grant No. 20120032110065 (Z.Q.L.), and by the Taiwan Ministry of Science and Technology through Grant No. NSC 103-2112-M-009-017-MY3 and the MOE ATU Plan (J.J.L.).

-
- * Electronic address: zhiqingli@tju.edu.cn
† Electronic address: jjlin@mail.nctu.edu.tw
- ¹ I. S. Beloborodov, A. V. Lopatin, V. M. Vinokur and K. B. Efetov, *Rev. Mod. Phys.* **79**, 469 (2007).
 - ² Y. J. Zhang, Z. Q. Li, and J. J. Lin, *Phys. Rev. B* **84**, 052202 (2011).
 - ³ Y. N. Wu, Y. F. Wei, Z. Q. Li, and J. J. Lin, *Phys. Rev. B* **91**, 104201 (2015).
 - ⁴ M. Reghu, C. O. Yoon, C. Y. Yang, D. Moses, P. Smith, A. J. Heeger and Y. Cao, *Phys. Rev. B* **50**, 13931 (1994).
 - ⁵ B. Abeles, H. L. Pinch and J. I. Gittleman, *Phys. Rev. Lett.* **35**, 247 (1975).
 - ⁶ R. W. Simon, B. J. Dalrymple, D. Van Vechten, W. W. Fuller and S. A. Wolf, *Phys. Rev. B* **36**, 1962 (1987).
 - ⁷ Y. H. Lin, Y. C. Sun, W. B. Jian, H. M. Chang, Y. S. Huang and J. J. Lin, *Nanotechnology* **19**, 045711 (2008).
 - ⁸ C. A. Neugebauer and M. B. Webb, *J. Appl. Phys.* **33**, 74 (1962).
 - ⁹ V. Ambegaokar, B. I. Halperin and J. S. Langer, *Phys. Rev. B* **4**, 2612 (1971).
 - ¹⁰ E. K. Sichel, J. I. Gittleman and P. Sheng, *Phys. Rev. B* **18**, 5712 (1978).
 - ¹¹ T. Chui, G. Deutscher, P. Lindenfeld and W. L. Mclean, *Phys. Rev. B* **23**, 6172 (1981).
 - ¹² E. Šimánek, *Solid State Commun.* **40**, 1021 (1981).
 - ¹³ C. J. Adkins, *J. Phys. C: Solid State Phys.* **15**, 7143 (1982).
 - ¹⁴ C. J. Adkins, *J. Phys.: Condens. Matter* **1**, 1253 (1989).
 - ¹⁵ M. Pollak and C. J. Adkins, *Philos. Mag. B* **65**, 855 (1992).
 - ¹⁶ O. Eatin-Wohlman, Y. Gefen and Y. Shapiro, *J. Phys. C* **16**, 1161 (1983).
 - ¹⁷ J. C. Phillips, *Phys. Rev. B* **64**, 035411 (2001).
 - ¹⁸ I. Balberg, J. Jedrzejewski and E. Savir, *Phys. Rev. B* **83**, 035318 (2011).
 - ¹⁹ A. L. Efros and B. I. Shklovskii, *J. Phys. C* **8**, L49 (1975).
 - ²⁰ A. L. Efros, *J. Phys. C: Solid State Phys.* **9**, 2021 (1976).
 - ²¹ R. Rosenbaum, *Phys. Rev. B* **44**, 3599 (1991).
 - ²² A. Bedoya-Pinto, J. Malindretos, M. Roeber, D. D. Mai, and A. Rizzi, *Phys. Rev. B* **80**, 195208 (2009).
 - ²³ A. Aharony, Y. Zhang, M. P. Sarachik, *Phys. Rev. Lett.* **68**, 3900 (1992).
 - ²⁴ P. Sheng, B. Abeles and Y. Arie, *Phys. Rev. Lett.* **31**, 44 (1973).
 - ²⁵ B. Abeles, P. Sheng, M. D. Coutts and Y. Arie, *Adv. Phys.* **24**, 407 (1975).
 - ²⁶ P. Sheng and J. Klafter, *Phys. Rev. B* **27**, 2583 (1983).
 - ²⁷ A. I. Yakimov, A. V. Dvurechenski, A. I. Nikiforov and A. A. Bloshkin, *Pis'ma Zh. Eksp. Teor. Fiz.* **77**, 445 (2003) [*JETP Lett.* **77**, 376 (2003)].
 - ²⁸ T. B. Tran, I. S. Beloborodov, X. M. Lin, T. P. Bigioni, V. M. Vinokur and H. M. Jaeger, *Phys. Rev. Lett.* **95**, 076806 (2005).
 - ²⁹ I. S. Beloborodov, A. V. Lopatin and V. M. Vinokur, *Phys. Rev. B* **72**, 125121 (2005).
 - ³⁰ Y. F. Wei and Z. Q. Li, *Appl. Phys. Lett.* **102**, 131911 (2013).
 - ³¹ Y. N. Wu, Z. Q. Li, and J. J. Lin, *Phys. Rev. B* **82**, 092202 (2010).
 - ³² R. Rosenbaum, *Phys. Rev. B* **44**, 3599 (1991).
 - ³³ P. Sheng and B. Abeles, *Phys. Rev. Lett.* **28**, 34 (1972).
 - ³⁴ C. Kittel, *Introduction to Solid State Physics*, 7th ed. (Wiley, New York, 1996).
 - ³⁵ Herbert B. Michaelson, *J. Appl. Phys.* **48**, 4729 (1977).
 - ³⁶ Z. Z. Yuan, D. S. Li, M. H. Wang, P. L. Chen and D. R. Gong, *Appl. Phys. Lett.* **92**, 121908 (2008).
 - ³⁷ D. Jousse, *Phys. Rev. B* **31**, 5335 (1985).
 - ³⁸ M. Kojima, H. Kato, A. Imai and A. Yoshida, *J. Appl. Phys.* **64**, 1902 (1988).
 - ³⁹ P. Sheng, and B. Abeles, *Phys. Rev. Lett.* **28**, 34 (1972).
 - ⁴⁰ P. Sheng, E. K. Sichel, and J. I. Gittleman, *Phys. Rev. Lett.* **40**, 1197 (1978).
 - ⁴¹ P. Sheng, *Phys. Rev. B* **21**, 2180 (1980).
 - ⁴² Z. H. Wang, M. S. Dresselhaus, G. Dresselhaus, K. A. Wang, and P. C. Eklund, *Phys. Rev. B* **49**, 15890 (1994).
 - ⁴³ M. Stiller, J. Barzola-Quiquia, M. Zoraghi, and P. Esquinazi, *Nanotechnology* **26**, 395703 (2015).
 - ⁴⁴ Y. H. Lin, S. P. Chiu, and J. J. Lin, *Nanotechnology* **19**, 365201 (2008).
 - ⁴⁵ Y. R. Lai, K. F. Yu, Y. H. Lin, J. C. Wu, and J. J. Lin, *AIP Adv.* **2**, 032155 (2012).
 - ⁴⁶ J. Ederth, P. Johnsson, G. A. Niklasson, A. Hoel, A. Hultker, P. Heszler, C. G. Granqvist, A. R. van Doorn, M. J. Jongerius, and D. Burgard, *Phys. Rev. B* **68**, 155410 (2003).
 - ⁴⁷ H. Xie and P. Sheng, *Phys. Rev. B* **79**, 165419 (2009).